PROCEEDINGS, 48th Workshop on Geothermal Reservoir Engineering
Stanford University, Stanford, California, February 6-8, 2023
SGP-TR-224

Deep Learning for Modeling Enhanced Geothermal Systems

Maruti Mudunuru[1], Bulbul Ahmmed[2], Luke Frash[2], and Rene Frijhoff[1]

[1]Pacific Northwest National Laboratory, Richland, WA 99362. [2]Los Alamos National Laboratory, Los Alamos, NM 87545

[1]Email address: maruti@pnnl.gov

Keywords: Enhanced Geothermal Systems, Geothermal Design Toolkit, Deep learning, Sensitivity Analysis, Techno-Economics.

ABSTRACT

Enhanced Geothermal Systems (EGS) offer a vast potential to expand the use of geothermal energy. Heat is extracted from this engineered system by injecting cold water into a subsurface fractures, which are in contact with hot dry rock, and brought back to surface through production wells. Creating EGS requires improving the natural permeability of hot crystalline rocks. To develop economically- viable EGS reservoirs, significant technical barriers (e.g., better stimulation technologies without adequate water and/or permeability) and non-technical barriers (e.g., land access, permitting, finance) must be overcome. *In this short conference paper, we present a workflow to address a part of this challenge – "How to develop economically viable EGS using existing technologies?".* Our workflow called the GeoThermalCloud (GTC) for EGS, leverages recent advances in machine learning, deep learning, and cloud computing. This GTC framework is open-source and available at https://github.com/SmartTensors/GeoThermalCloud.jl. The GTC framework provides trained deep learning (DL) models to estimate the undiscounted cashflow of a given EGS design scenario. The Geothermal Design Tool (https://github.com/GeoDesignTool/GeoDT.git), a fast and simplified multi-physics solver, is used to develop a database for training DL models. The database consists of EGS design parameters (inputs to DL model) and their undiscounted cashflow (output of DL model) in uncertain geologic systems. The EGS design parameters for constructing this training database are based on UtahFORGE but include the options of more wells and deeper depths. The DL models are trained by ingesting the EGS design parameters and estimating the corresponding undiscounted cashflow. Such an emulation allows us to screen various EGS designs quickly and identify good development strategies by coupling them with optimization techniques. Our preliminary results show promise in DL emulation of undiscounted cashflow. However, a lot more work is needed to improve the predictive capability of DL models (i.e., extensive hyperparameter tuning is necessary). This will be the primary focus of our future work.

1. INTRODUCTION

Enhanced Geothermal Systems (EGS) are engineered geothermal systems, which offer great potential for dramatically expanding the use of geothermal energy (Brown et al., 2012). In this engineered system, cold water is injected into hot dry rock and is allowed to flow through a fracture network. The resulting hot fluid is extracted from production wells to generate electricity. The U.S. Department of Energy's GeoVision report in 2019 estimates that more than 100GWe of economically viable power capacity is possible to extract from the southwestern basins (GeoVison, 2019 DOE-MYPP 2022, EarthShot Initiative, 2022). However, high upfront costs and long development timelines generally characterize geothermal resource development projects (Hamm et al., 2021). This can lead to lengthy investment payback periods relative to many other utility-scale power generation projects (e.g., wind, solar). Moreover, projects employing new EGS designs and stimulation technologies to harness this renewable resource and produce usable power can have higher risks (Becker et al., 2018). To overcome this challenge of reducing costs and improving economics for geothermal projects, we need to understand feasible and non-feasible EGS designs better. Specifically, a detailed techno-economic analysis is required to successfully expand and accelerate EGS deployment in the western U.S (DOE-MYPP, 2022; Sec-2). A workflow that combines geothermal data, multi-physics process models, and economics to assess good and bad EGS design parameters will allow us to overcome such a challenge (Sec-2.4 and Sec-2.5 in DOE-GTO MYPP, 2022). Recent deep learning (DL) advances have shown promise in developing such a workflow (Okoroafor et al., 2022). In this short conference paper, we provide a DL methodology to create a non-linear mapping between EGS design parameters and the undiscounted cashflow of the resource. This DL methodology that we are developing will be made available to the geothermal community through our open-source machine learning framework called GeoThermalCloud (GTC), available at https://github.com/SmartTensors/GeoThermalCloud.jl.

The outline of our paper is as follows: Section 2 provides the methods involved in developing the GTC framework, training database using GeoDT, and workflow to develop scalable deep learning models. Section 3 provides the results describing the training database, sensitivity analysis, and preliminary results from DL model training. Conclusions are drawn in Section 4.

2. METHODS

In this section, we describe the high-level framework of GTC for EGS, training database based on GeoDT, and proposed DL methodology for emulating undiscounted cashflow.

2.1 GeoThermalCloud for EGS

The GTC framework (https://github.com/SmartTensors/GeoThermalCloud.jl) is developed to enhance data collection during exploration and optimize the EGS design during resource development scenarios and operations (Vesselinov et al., 2021; Mudunuru et al., 2022). Figure 1 summarizes our GTC framework. The proposed framework consists of two components (1) GTC for exploration and (2) GTC

for resource development. The GTC for the exploration component (Ahmmed and Vesselinov, 2022) enhances the play fairway analysis datasets and estimates the geothermal resource parameter potential. This exploration component is built using NMFk, an unsupervised ML method available in the SmartTensors AI platform (https://github.com/SmartTensors/NMFk.jl). The GTC for exploration component is extensively tested on various play fair analysis datasets curated from DOE's Geothermal Data Repository. Once the GTC for exploration identifies potential resources within a given region, then EGS design scenarios are explored at these promising sites. The second component, GTC for resource development, which is currently under development, achieves this goal of optimizing EGS designs to find and rank the most promising site through undiscounted cashflow. This GTC for resource development utilizes recent advances in deep learning (e.g., deep neural networks) to develop a non-linear mapping between inputs (i.e., EGS design parameters) and outputs (i.e., thermal power production, undiscounted cashflow). Detailed sensitivity analysis is performed to identify EGS parameters and rank them based on undiscounted cashflow. Using a simple economics model, the emulated DL models are then used in an optimization framework to assess the resources that are viable for thermal power production (Frash et al., 2013).

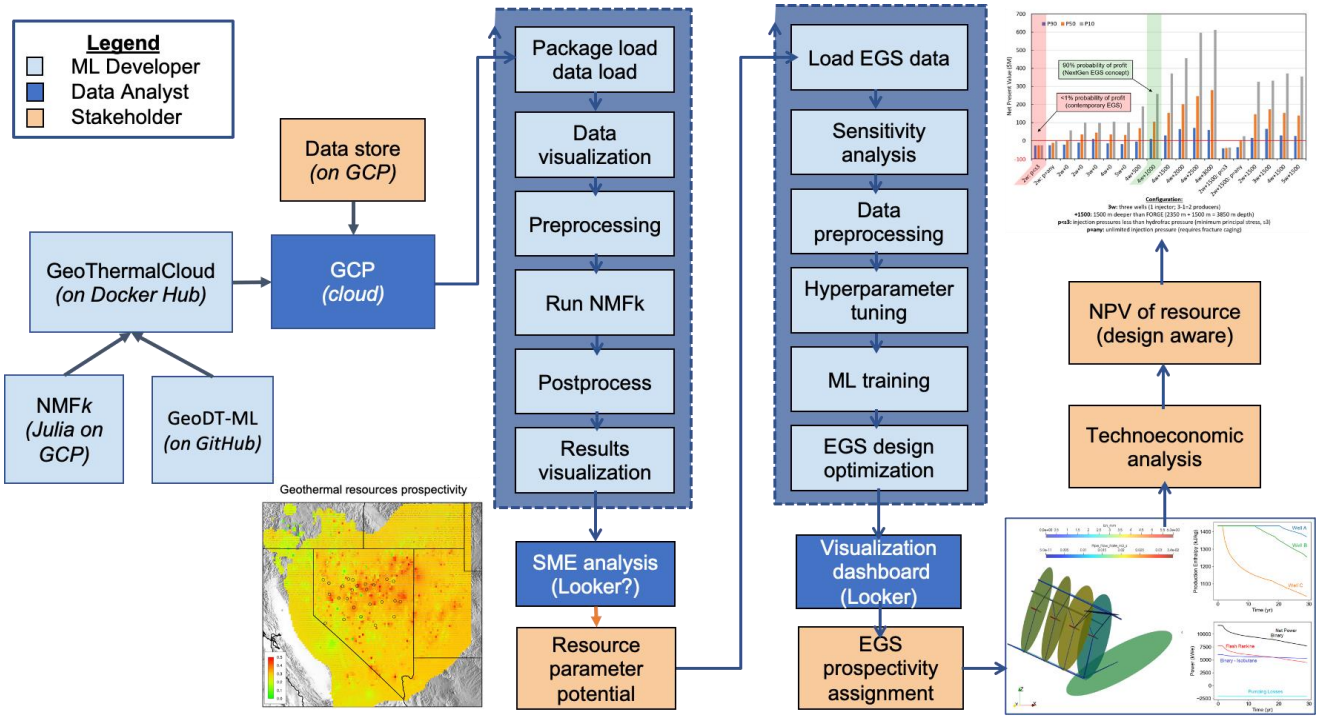

Figure 1: This figure describes the GTC framework and its two components – exploration and development. The exploration component analyzes and curates play fairway analysis datasets to find the resource potential within a region. The resource component builds on these potential maps and assesses the EGS prospectivity to find and rank the most promising sites for further analysis.

2.2 Training database using GeoDT

The GeoDT (https://github.com/GeoDesignTool/GeoDT.git) is a fast, simplified multi-physics solver to evaluate EGS designs in uncertain geologic systems (Frash, 2021; Frash, 2022; Frash et al., 2022). Figure 2 shows a schematic of GeoDT workflow to estimate EGS outputs such as thermal power production and associated economics (e.g., undiscounted cashflow). In GeoDT, a 3D network of intersecting wells and fractures are modeled as pipes and nodes, in which fluid flow is solved. Transient thermal power production values depend on fluid enthalpy, rock conductivity, and stored energy change over time. The combined single-flash Rankine and isobutane binary cycle models are used in estimating electrical power generation. In the final step, the undiscounted cashflow is computed based on geothermal cost estimation tools, electricity sales, and a simple earthquake cost model. Table 1 shows the range of system parameters that are changed to generate this training database of realizations. Table 2 provides the summary of cost terms in the economics model of GeoDT. DL models are built on this training database to emulate undiscounted cashflow. In our study, a total of 4078 realizations are generated, which is split into 80% training, 10% validation, and 10% testing. When the DL model identifies a promising EGS design, it can then be further investigated in greater detail. For example, we can use high-fidelity process models and simulation codes such as PFLOTRAN (Lichtner et al., 2015) to explore promising EGS scenarios. This study does not include the use of high-fidelity codes.

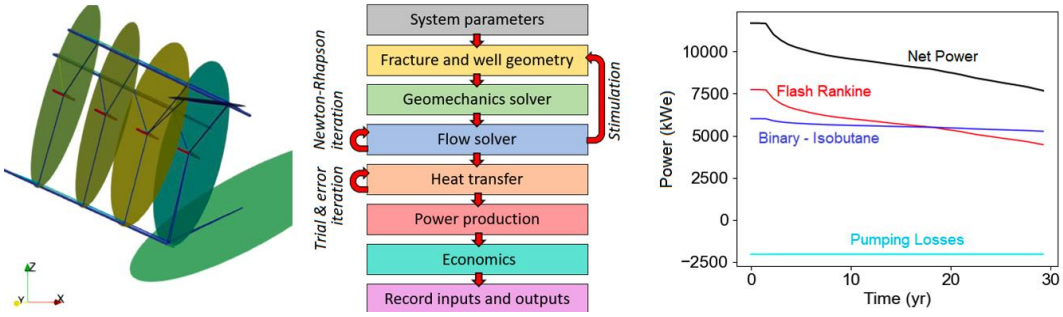

Figure 2: A schematic of GeoDT workflow to generate a training database for DL models. System parameters are varied and given to various solvers. These solvers estimate power production and economics needed for training DL models.

2.3 Proposed DL methodology

In this subsection, we discuss our proposed methodology to develop DL models. Figure 3 shows the proposed approach to curate the training database and create emulators. First, the GeoDT realizations are pre-processed and standardized for DL training. This standardization is necessary because deep neural networks (Samek et al., 2021) learn from the training data, and the learning outcome for EGS design scenarios heavily depends on how the data is curated. Standard scaling is selected to standardize the data among the seven different pre-processors. We will compare the other six pre-processor scalars in our future work on DL model performance. Standard scaling curates the data to remove the mean and scale it to unit variance, resulting in standard normal distributed data. This curated data is given as input to deep neural networks, which are trained on multiple cores available on high-performance computing machines (HPC). This AI training at scale is performed in parallel, allowing us to train and tune various deep neural networks in minimal time. We combine python and AI modules such as mpi4py, multiprocessing, parallel hdf5, and TensorFlow to achieve this training at scale. The performance of the trained DL models is compared using the validation loss, and a tuned model is then selected. This hyperparameter tuning is computationally intensive and requires a lot of HPC resources.

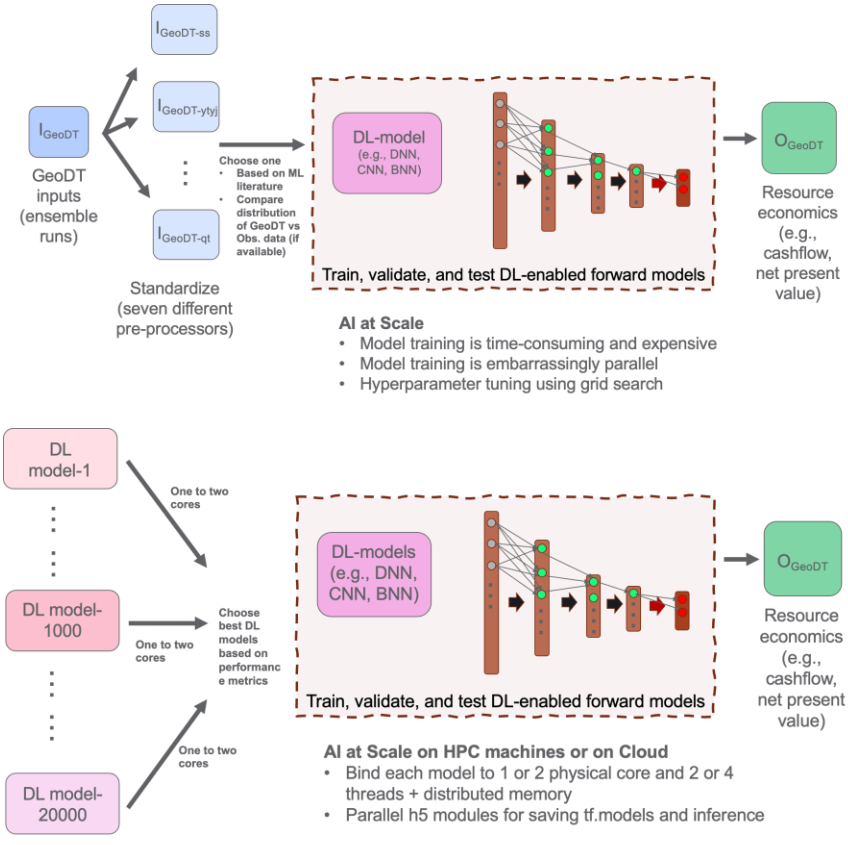

Figure 3: This figure shows the proposed DL methodology to train neural networks at scale on high-performance computing machines or the cloud (e.g., GCP, AWS, Azure). First, the EGS design parameters from GeoDT are curated and given as input to the deep neural network. The output of this neural network is the undiscounted cashflow. Then, various such deep neural networks are trained on HPC/cloud to tune the hyperparameters to find reasonably accurate emulators.

Table 1: This table provides the EGS design input parameters used in GeoDT conditioned on FORGE site.

DoF	Category	Variable	Parameter	Unit	Min Value	Nominal value	Max Value	Uncertainty (±)	Distribution	Source	Source	Notes
1	Solver Setup	size	Domain size (i.e., cubic side length)	m		1500			-	-	-	
1	Site	ResDepth	Nominal reservoir depth	m	4000		10000		Uniform	Tester et al., 2006	Tester et al., 2006	
1	Site	ResGradient	Geothermal gradient	K/km	35		55		Uniform	Bearsdmore and Cull, 2001	Bearsdmore, G.R. and Cull, J.P	
1	Site	ResRho	Rock density	kg/m3	2550		2850		Uniform	Waples and Waples, 2004	Waples, D.W. and Waples, J.S.	
1	Site	ResKt	Rock thermal conductivity	W/mK	2.2		2.8		Uniform	Bearsdmore and Cull, 2001	Bearsdmore, G.R. and Cull, J.P	
1	Site	ResSv	Rock volumetric specific heat capacity	kJ/m3K	1850		2150		Uniform	Waples and Waples, 2004	Waples, D.W. and Waples, J.S.	
1	Site	AmbTempC	Ambient surface temperature	C	5		30		Uniform	Temperate climates	Temperate climates	
1	Site	AmbPres	Ambient surface pressure	MPa		0.101			-	Temperate climates	Temperate climates	
1	Stress	ResE	Rock elastic modulus	GPa	50		110		Uniform	Carmichael, 1982	Carmichael, R. (1982) Revival:	
1	Stress	Resv	Rock Poisson's ratio	m/m	0.15		0.35		Uniform	Carmichael, 1982	Carmichael, R. (1982) Revival:	
1	Stress	Ks3	Minimum lateral earth pressure coefficient	Pa/Pa	0.5		0.9		Uniform	Zoback, 2018	Zoback, M.D. (2018) Reservoir	
1	Stress	Ks2	Intermediate earth pressure coefficient	Pa/Pa	0.6		1.2		Uniform	Zoback, 2018	Zoback, M.D. (2018) Reservoir	
0	Stress	s3Azn	Minimum stress azimuth	deg		0.1		5	Normal	"North"	"North"	
0	Stress	s3Dip	Minimum stress dip	deg		0.1		5	Normal	"North"	"North"	
1	Fracture	fNum	Fracture set 1 count	fractures	0		40		Uniform	Sub-perpendicular to wells	Sub-perpendicular to wells	
2	Fracture	fDia	Fracture set 1 diameter	m	50		1000		Uniform	Sub-perpendicular to wells	Sub-perpendicular to wells	
2	Fracture	fStr	Fracture set 1 strike	deg	112		158		Uniform	Sub-perpendicular to wells	Sub-perpendicular to wells	
2	Fracture	fDip	Fracture set 1 dip	deg	67		113		Uniform	Sub-perpendicular to wells	Sub-perpendicular to wells	
1	Fracture	fNum	Fracture set 2 count	fractures	0		40		Uniform	Sub-parallel to wells	Sub-parallel to wells	
2	Fracture	fDia	Fracture set 2 diameter	m	50		1000		Uniform	Sub-parallel to wells	Sub-parallel to wells	
2	Fracture	fStr	Fracture set 2 strike	deg	22		67		Uniform	Sub-parallel to wells	Sub-parallel to wells	
2	Fracture	fDip	Fracture set 2 dip	deg	67		113		Uniform	Sub-parallel to wells	Sub-parallel to wells	
1	Fracture	fNum	Fracture set 3 count	fractures	0		40		Uniform	Sub-parallel to wells conjugate set	Sub-parallel to wells conjugate	
2	Fracture	fDia	Fracture set 3 diameter	m	50		1000		Uniform	Sub-parallel to wells conjugate set	Sub-parallel to wells conjugate	
2	Fracture	fStr	Fracture set 3 strike	deg	90		270		Uniform	Sub-parallel to wells conjugate set	Sub-parallel to wells conjugate	
2	Fracture	fDip	Fracture set 3 dip	deg	-22		23		Uniform	Sub-parallel to wells conjugate set	Sub-parallel to wells conjugate	
3	Scaling	gamma	Shear displacement-length coefficient	m/m	0.001	0.01	0.063	0.01	Truncated Lognorr	Frash et al., 2021	Frash et al., 2021	
1	Scaling	n1	Shear displacement-length exponent	-		1			Uniform	Frash et al., 2021	Frash et al., 2021	
3	Scaling	a	Shear displacement-dilation coefficient	m/m	0	0.2	0.8	0.2	Truncated Normal	Frash et al., 2021	Frash et al., 2021	
2	Scaling	b	Shear displacement-dilation exponent	-		1			Uniform	Frash et al., 2021	Frash et al., 2021	
2	Scaling	N	Witherspoon factor	m/m	0	0.6	2	0.6	Special	Frash et al., 2021	Frash et al., 2021	
3	Scaling	alpha	Fracture compressibility	1/MPa	2.00E-09	2.90E-08	1.00E-07	2.90E-08	Truncated Normal	Frash et al., 2021	Frash et al., 2021	
2	Scaling	bh	Default hydraulic aperture	m	0.00005	0.0005	0.002	0.0005	Truncated Normal	Frash et al., 2021	Frash et al., 2021	
1	Solver Setup	bh_min	Minimum hydraulic aperture	m		0.00005			-	-	-	
1	Solver Setup	bh_max	Maximum hydraulic aperture	m		1			-	-	-	
2	Site	bh_bound	Boundary hydraulic aperture	m	0.0001		0.002		Uniform	-	-	
2	Scaling	f_roughness	Fracture roughness	-	0.7		1		Uniform	-	-	
1	Well	w_count	Well count	wells	1		6		Uniform	-	-	
1	Well	w_spacing	Well spacing	m	200		1100		Uniform	-	-	
1	Well	w_length	Well length	m	800		1200		Lognormal	-	-	
1	Well	w_azimuth	Well azimuth	deg	0		90		Uniform	-	-	
1	Well	w_dip	Well dip	deg	0		90		Uniform	-	-	
1	Well	w_proportion	Well proportion	deg	0.4		1		Uniform	-	-	
1	Well	w_phase	Well phase	deg	0		360		Uniform	-	-	
1	Well	w_toe	Well toe	deg	-15		15		Uniform	-	-	
1	Well	w_skew	Well skew	deg	-15		15		Uniform	-	-	
1	Well	w_intervals	Well intervals	zones	1		10		Uniform	-	-	
1	Well	ra	Casing inner radius	m	0.1		0.23		Uniform	Oil County Tubular Goods, 2020	https://www.susmar.fi/pdc/in	
1	Well	rb	Casing outer radius	m		ra + 0.013			-	-	https://www.susmar.fi/pdc/in	
1	Well	rc	Borehole radius	m		rb + 0.013			-	-	https://www.susmar.fi/pdc/in	
0	Well	rgh	Hazen-Williams friction coefficient	-		80			-	Jeppson, 1974	Jeppson, R.W. (1974) Steady fl	
1	Well	CemKt	Cement thermal conductivity	W/mK		2			-	Asadi et al., 2018	Asadi, I., Shafigh, P., Hassan, Z.	
1	Well	CemSv	Cement volumetric specific heat capaci	kJ/m3K		2000			-	Kodur, 2014	Kodur, V. (2014) Properties of	
0	Power	GenEfficiency	Electrical generator efficiency	%		0.85			-	Electropaedia	https://www.mpoweruk.com/	
0	Power	LifeSpan	Project lifespan	yr		20.5			-	Vitaller et al., 2020	Vitaller, A.V., Angst, U.M., Else	
0	Solver Setup	TimeSteps	Thermal analysis timesteps	steps		41			-	-	-	
1	Power	p_whp	Power plant inlet pressure	MPa		1			-	-	https://thermopedia.com/cor	
0	Power	Tinj	Injection temperature	C		95			-	-		
1	Well	H_ConvCoef	Borehole thermal convection coefficien	kW/m2K		3			-	Kosky et al., 2013	Kosky, P., Balmer,	*Full CFD +
0	Solver Setup	dT0	Initial step temperature change	K		10			-	-	Used to stabilize early time the	
0	Solver Setup	dE0	Initial step thermal energy change	kJ/m2		500			-	-	Used to stabilize early time the	
0	Solver Setup	PoreRho	Water density for flow analysis	kg/m3		980			-	Cooper, J.R. and Dooley, R.B. (2007) Revised relea	Cooper, J.R. and Dooley, R.B. (	
0	Solver Setup	Poremu	Water dynamic viscosity	cP		0.25			-	Huber, M.L., Perkins, R.A., Laesecke, A., Friend, D.	Huber, M.L., Perkins, R.A., Laes	
0	Well	perf	Perforation count per injection interval	perfs		1			-	-	-	*Solver req
0	Solver Setup	r_perf	Perforation radus	m		50			-	-	-	*Initial hyd
1	Well	dPp	Production well pressure change from a	MPa	-10		2		Uniform	-	-	
0	Solver Setup	dPi	Pressure increment	MPa		0.1			-	Savitski and Detournay (2002) Propagation of a p	Savitski and Detou	*This was fo
0	Solver Setup	stim_limit	Number of stimulation iterations before	pressure increment		5			-	-	-	
1	Stimulation	Qstim	Stimulation flow rate	m3/s	0.02		0.08		Uniform	Industry quote for UtahFORGE	Industry quote for	*Schlumbe
1	Stimulation	Vstim	Stimulation volume	m3	9		1700		Uniform	Industry quote for UtahFORGE	Industry quote for UtahFORGE	
0	Solver Setup	bval	b-value (Gutenberg Richter)			1			-	Gutenberg-Richter	Gutenberg-Richter	
2	Fracture	phi	Fracture friction angle	-	20		55		Uniform	Lab tests on range of rock types	Lab tests on range of rock type	
2	Fracture	mcc	Fracture cohesion	MPa	0		20		Uniform	Lab tests on range of rock types	Lab tests on range of rock type	
2	Site	hfmcc	Hydraulic fracture cohesion	MPa	0.1		0.3		Uniform	Lab tests on range of rock types	Lab tests on range of rock type	
2	Site	hfphi	Hydraulic fracture friction angle	deg	15		35		Uniform	Lab tests on range of rock types	Lab tests on range of rock type	
1	Stimulation	Qinj	Circulation injection flow rate	m3/s	0.005		0.05		Uniform	-	-	*Value per
0	Site	BH_P	Reservoir pore pressure	MPa	38.5		96.1		-	-	-	*BH_P = Po
0	Site	BH_T	Reservoir temperature	K	422		849		-	-	-	*BH_T = Res
0	Stress	ResG	Rock shear modulus	GPa	18.6		47.7		-	-	-	*G = E/2(1-v
0	Stress	s1	Overburden stress	MPa	101		278		Uniform	-	-	*s1 = ResRh
0	Stress	s2	Intermediate stress	MPa	83		311		Uniform	-	-	*s2 = (s1-BH
0	Stress	s3	Minimum stress	MPa	72		257		Uniform	-	-	*s3 = (s1-BH
0	Scaling	Porek	Matrix permeability	mD					Uniform	-	-	
0	Scaling	Frack	Fracture permeability	mD					Uniform	-	-	
0	Stimulation	sand	Frac sand concentration						Uniform			*not curren
0	Stimulation	leakoff	Carter leakoff coefficient						Uniform			*not curren
84	degrees of freedom											
18	controllable design parameters											

	Precursor inputs			Category	Parameter	Parameter	Unit	Mean value	Min Value	Max Value		Informational
	Model parameters			Power	Pout	Rankine electrical power - time variable	kW					High priority decision point
	Model controls			Power	hpro	Production enthalpy - time variable	kJ/kg					Low priority decision point
	Static inputs			Power	dhout	Extracted thermal power - time variable	kJ/s					Quality control
	Covariants			Power	mpro	Production mass flow rate	kg/s					Missing but needed
				Hazard	max_quake	Maximum induced earthquake magnitude	Mw					
	Controllable design decisions			Efficiency	recovery	Production rate / Injection rate	ratio					
	Cannot be measured in-situ			Efficiency	qgain	Boundary inflow rate	m3/s					
	Intermediate calculations			Efficiency	qleak	Boundary outflow rate	m3/s					
				Efficiency	qpro	Cumulative production rate	m3/s					
				Efficiency	qinj	Cumulatiove injection rate	m3/s					
				Error indication	-	Solver error (e.g., no interwell flow)	-					
				Efficiency	pinj	Pressure of injected fluid	MPa					
				Efficiency	hinj	Enthalpy of injected fluid	kJ/kg					
				Intercepts	ixint	Number of fractures intercepting injectors	fractures					
				Intercepts	pxint	Number of fractures intercepting producers	fractures					
				Intercepts	hfstim	Number of stimulated hydraulic fractures	fractures					
				Intercepts	nfstim	Number of stimulated natural fracutres	fractures					

Table 2: This table provides a summary of cost terms in the economics model of GeoDT. We didn't use discount rates in our calculations as it is challenging to forecast the electricity discounts for renewables.

Parameter	Unit	Value	Uncertainty	Reference
Electricity sales per kilowatt-hour	USD/kWh	0.1372	-0.056/ +0.166	EIA, 2022
Drilling cost per length	USD/m	2763	+/- 536	Lowry et al., 2017
Drill pad cost	kUSD	590	-590/ + 2000	Lowry et al., 2017
Power plant cost	USD	2026	+/- 373	GETEM (Entingh et al., 2012)
Exploration cost per depth	USD/m	2683	+/- 472	GETEM (Entingh et al., 2012)
Operating cost per kilowatt-hour	USD/kWh	0.0365	+/- 0.0079	GETEM (Entingh et al., 2012)
Seismic risk coefficient	USD	0.0002	10^{-8} to 10^{-3}	Frash et al., 2013
Seismic risk exponent	1/MW	5.0	2.0 to 5.5	Frash et al., 2013

3. RESULTS

This section provides preliminary results on the training database, sensitivity analysis, and DL model predictions. Figure 4 shows the outputs produced by GeoDT for 4078 realizations. These time-series outputs include normalized production enthalpy and thermal power and are used in estimating undiscounted cashflow. The training data is normalized for EGS design scenario analysis rather than the absolute values (please see disclaimer section). These figures show that a decrease in well enthalpy may be beneficial to producing more power output overall. This reduction in enthalpy can be attributed to the mechanism of greater heat flux (i.e., power transfer) from more significant thermal gradients (i.e., thermal drawdown).

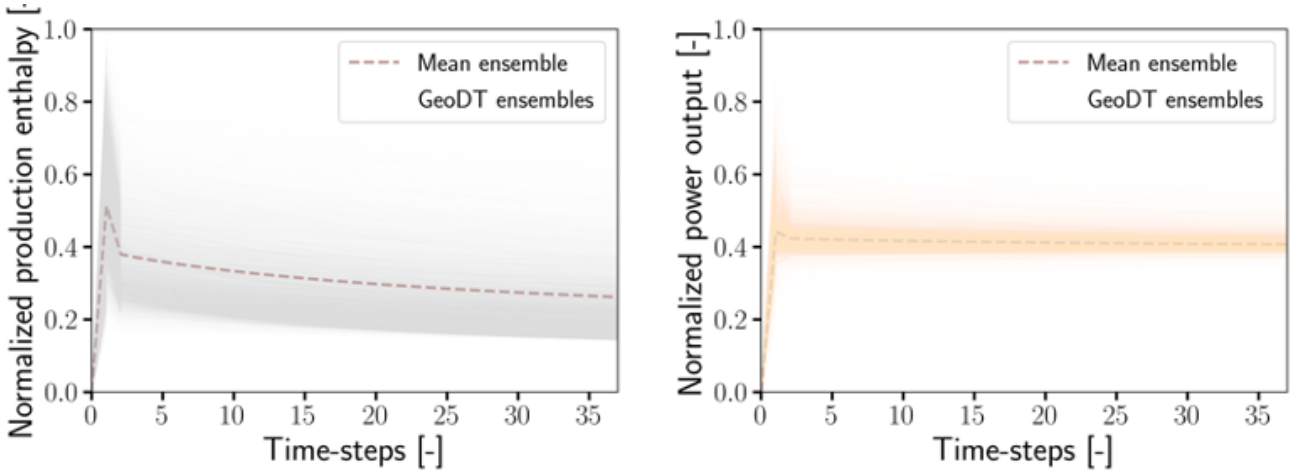

Figure 4: This figure shows normalized production enthalpy and power output time-series obtained from GeoDT simulations.

Figure 5 shows the sensitivity analysis of EGS design parameters used in GeoDT with respect to undiscounted cashflow. Sensitivity analysis is performed using two different approaches, F-test and mutual information (MI). F-test is a univariate linear regression tests

returning F-statistic and p-values. It provides insights on the linear dependency of a given EGS design parameter with respect to undiscounted cashflow, thereby allowing us to identify potentially predictive design parameters for DL model training for undiscounted cashflow. On the other hand, mutual information provides insights on non-linear dependency between EGS design parameters and undiscounted cashflow. The MI between a EGS design parameter and undiscounted cashflow is a non-negative value and is equal to zero if and only if two variables are independent, and higher values mean higher non-linear dependency. From F-test sensitivity analysis it is evident that flow rate (Qinj, Vinj) shows strong linear dependency as expected in a simplified physics model (Brown et al. 2012). The MI results show that minimum stress (s3), injection temperature (Tinj), hydrualic fracture friction angle (Hfphi), minimum stress dip (s3Dip), geothermal gradient (ResGradient), minimum lateral earth pressure coefficient (Ks3), rock density (ResRho), rock volumetric heat capacity (ResRv), and nominal reservoir depth (ResDepth), have strong non-linear dependency.

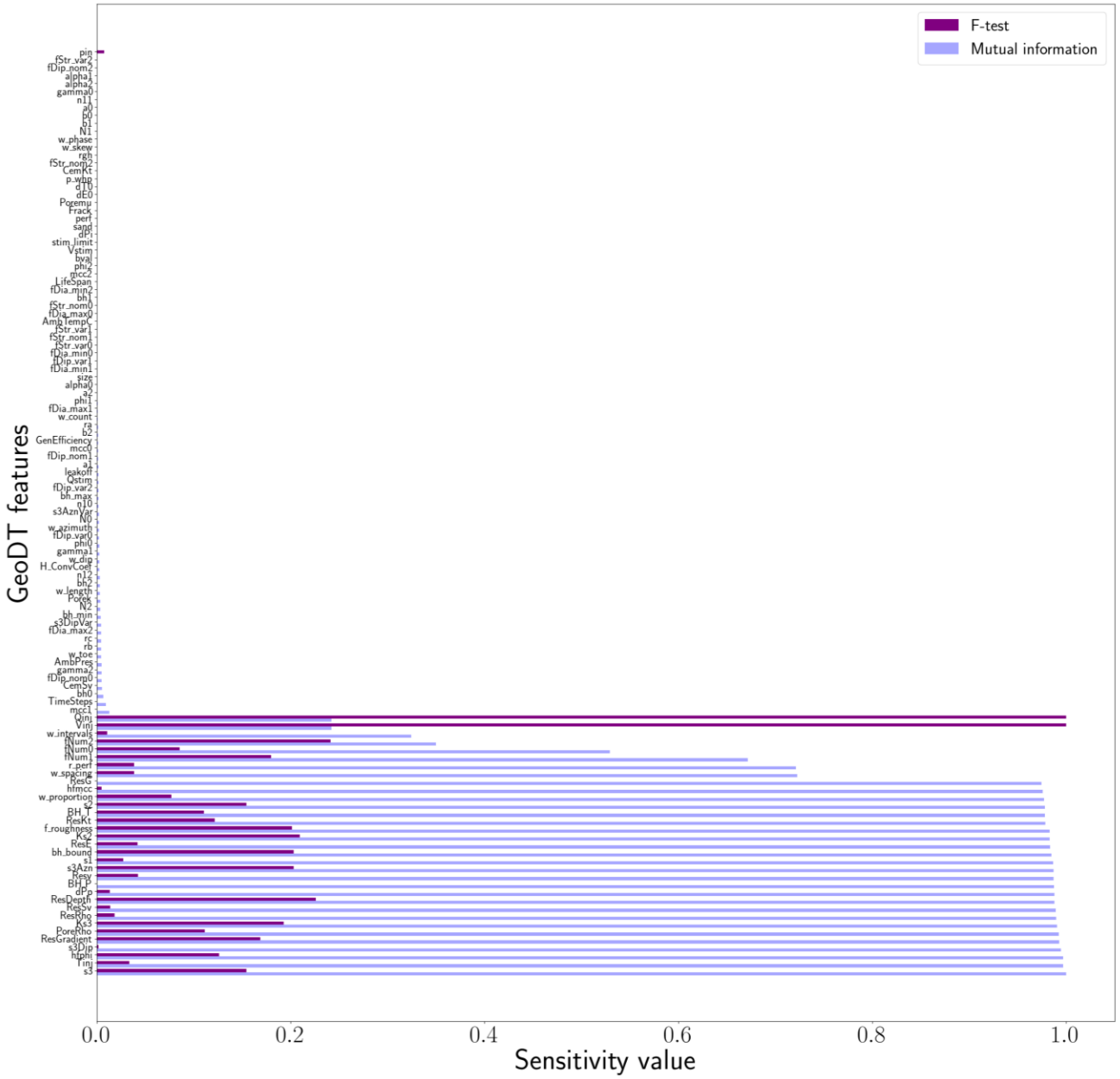

Figure 5: This figure provides a bar plot of the sensitivity values for each GeoDT feature or parameter.

Figure 6 shows the results of DL training and prediction. This trained deep neural network model has three hidden layers, with neurons = [1000, 500, 250] in each of these layers. Leaky ReLU is used as an activation function with alpha value = 0.1. The dropout value, which allows for minimizing over-fitting during the training process, is assigned a value of 0.1. The total number of epochs for training is equal to 100. Batch size, which is the number of training samples that a DL model sees for each iteration in an epoch is equal to 64. The resulting DNN has approximately 750K trainable weights. The loss vs. epochs results show that the lower learning rate combined with dropout reduces over-fitting. Training loss decreases; validation loss declines for over half of the epochs and then rises slowly. This training and validation loss trend shows that the DL model tends to overfit beyond 100 epochs. The one-to-one plots from training,

validation, and test datasets show that the DL model can perform reasonably well for low undiscounted cashflow. But for higher values of undiscounted cashflow, the DL model performance is not satisfactory as it deviates considerably from the one-to-one line in both test and validation datasets. Hyperparameter tuning is needed to find better DNNs that show improved performance for higher undiscounted cashflow. The non-sensitive EGS parameters may also contribute to the reduced performance. Additional analysis is required to use only the sensitivity parameters to train DL models, which is our next step.

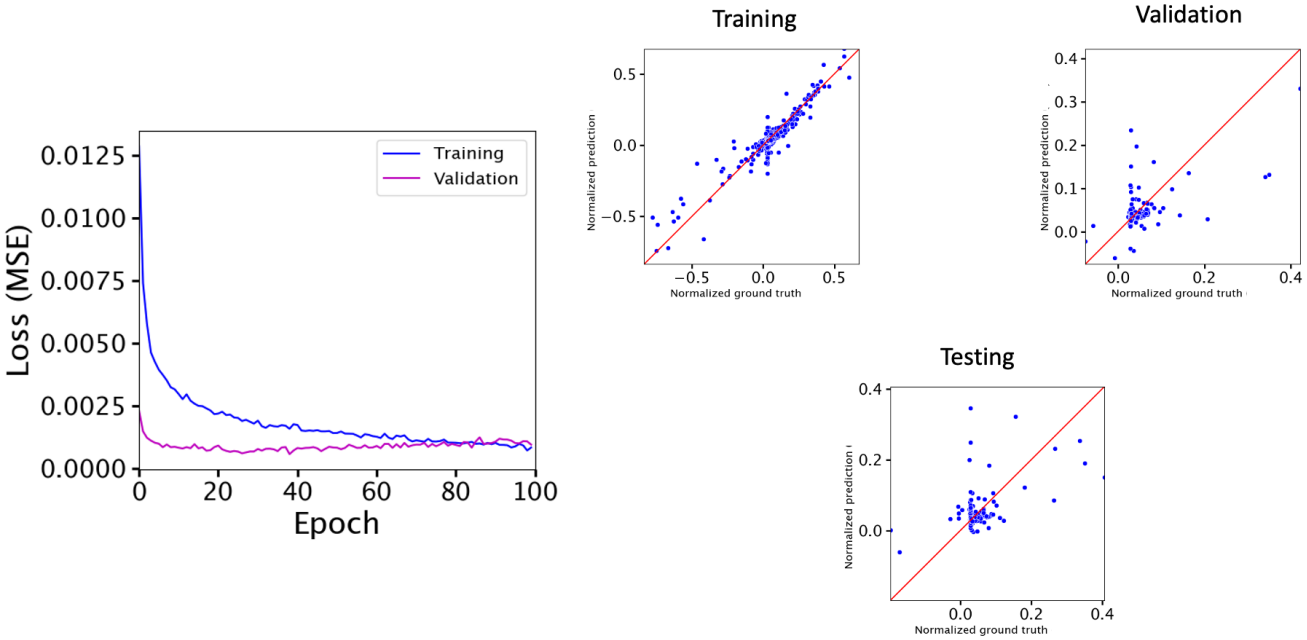

Figure 6: This figure provides the DL model training loss and one-to-one plots for training, validation, and test datasets.

4. CONCLUSIONS

We developed a DL workflow in this study to estimate undiscounted cashflow from EGS design parameters. The database for DL model training is developed using GeoDT, a multi-physics solver. Sensitivity analysis using F-test and mutual information is performed on this database to gain insights into the GeoDT parameters. This preliminary sensitivity analysis showed that injection rate, temperature, and stress factors influence the undiscounted cashflow. The DL models are developed using deep neural networks, which map GeoDT features to undiscounted cashflow. Our preliminary results showed that DL models can reasonably predict lower undiscounted cashflow but show challenges in predicting higher undiscounted cashflow. Therefore, better predictive DNNs are needed to improve the accuracy of undiscounted cashflow estimation. Our next step is to perform extensive hyperparameter tuning and sensitivity-analysis-guided DL model training to achieve this. This extensive hyperparameter tuning allows us to find better DNNs with informative/sensitive GeoDT features. In our future work, we will explore coupling DL models trained on GeoDT thermal power production with advanced techno-economic analysis modules such as GEOPHIRES (https://github.com/NREL/GEOPHIRES-v2). Upon satisfactory performance of DNN and hyperparameter tuning, we will make the GeoDT training database, python scripts, Jupyter notebooks, and pre-trained DL models available through GeoThermalCloud https://github.com/SmartTensors/GeoThermalCloud.jl. Once our DL model performs with reasonably good accuracy, we will explore the EGS design parameters (as listed in Table-1) that contribute to higher undiscounted cashflow value.

DISCLAIMER

The training database using GeoDT employs very-high estimates of seismic risk and an unproven new muti-physics model. The actual FORGE project uses lower injection rates, lower injection volumes, closer well spacing, shallower depths, and seismicity mitigation measures that our model needs to include. In short, this work is not a prediction for the UtahFORGE project.

ACKNOWLEDGEMENTS

This research is based upon work supported by the U.S. Department of Energy's (DOE) Office of Energy Efficiency and Renewable Energy (EERE) under the Geothermal Technology Office (GTO) Machine Learning (ML) for Geothermal Energy funding opportunity, Award Number DE-EE-3.1.8.1. Los Alamos National Laboratory is operated by Triad National Security, LLC, for the National Nuclear Security Administration of the U.S. Department of Energy (Contract No. 89233218CNA000001). All the codes, pre-trained models, and database will be made available at https://github.com/SmartTensors/GeoThermalCloud.jl.

REFERENCES

Ahmmed, B. and Vesselinov, V.V., 2022. Machine learning and shallow groundwater chemistry to identify geothermal prospects in the Great Basin, USA. Renewable Energy, 197, pp.1034-1048.

Beckers, K.J. and McCabe, K., 2018. Introducing GEOPHIRES v2. 0: updated geothermal techno-economic simulation tool (No. NREL/CP-5500-70856). National Renewable Energy Lab.(NREL), Golden, CO (United States).

Brown, D.W., Duchane, D.V., Heiken, G. and Hriscu, V.T., 2012. Mining the earth's heat: hot dry rock geothermal energy. Springer Science & Business Media.

Energy EarthShots, DOE Office of Policy, https://www.energy.gov/policy/energy-earthshots-initiative, 2022

Enhanced Geothermal Shot, An Energy EarthShot Initiative by DOE-GTO, https://www.energy.gov/eere/geothermal/enhanced-geothermal-shot

GTO Multi-Year Program Plan (FY 2022-2026), https://www.energy.gov/sites/default/files/2022-02/GTO%20Multi-Year%20Program%20Plan%20FY%202022-2026.pdf, 2022.

GeoVision Report, Harnessing the Heat Beneath Our Feet, DOE-GTO, 2019.

Frash, L.P.: Optimized Enhanced Geothermal Development Strategies with GeoDT and Fracture Caging, Proceedings, 47th Workshop on Geothermal Reservoir Engineering, Stanford University, Stanford, CA (2022).

Frash, L.P.: Geothermal Design Tool (GeoDT), Proceedings, 46th Workshop on Geothermal Reservoir Engineering, Stanford University, Stanford, CA (2021).

Frash, L.P., Fu, P., Morris, J., Gutierrez, M., Neupane, G., Hampton, J., Welch, N., Carey, J.W., Kneafsey, T.: Fracture Caging to Limit Induced Seismicity, Geophysical Research Letters, 48(1), e2020GL090648 (2020).

Frash, L.P., Li, W., Meng, M., Carey, J.W., Sweeney, M.: Enhanced Geothermal System Design Using GeoDT and Fracture Caging — EGS Collab Stimulation Prediction Study, Proceedings, 56th US Rock Mechanics/Geomechanics Symposium, Santa Fe, NM (2022).

Frash, L.P., Carey, J. W., Ahmmed, B., Meng, M., Sweeney, M., Bijay, K. C., Iyare, U., Madenova, Y., Let's Make Enhanced Geothermal Systems Work, Proceedings, 48th Workshop on Geothermal Reservoir Engineering, Stanford University, Stanford, CA (2023).

Hamm, S.G., Anderson, A., Blankenship, D., Boyd, L.W., Brown, E.A., Frone, Z., Hamos, I., Hughes, H.J., Kalmuk, M., Marble, A. and McKittrick, A.M., 2021. Geothermal Energy R&D: An Overview of the US Department of Energy's Geothermal Technologies Office. Journal of Energy Resources Technology, 143(10), p.100801.

Lichtner, P.C., Hammond, G.E., Lu, C., Karra, S., Bisht, G., Andre, B., Mills, R. and Kumar, J., 2015. PFLOTRAN user manual: A massively parallel reactive flow and transport model for describing surface and subsurface processes (No. LA-UR-15-20403). Los Alamos National Lab.(LANL), Los Alamos, NM (United States); Sandia National Lab.(SNL-NM), Albuquerque, NM (United States); Lawrence Berkeley National Lab.(LBNL), Berkeley, CA (United States); Oak Ridge National Lab.(ORNL), Oak Ridge, TN (United States); OFM Research, Redmond, WA (United States).

Mudunuru, M.K., Vesselinov, V.V. and Ahmmed, B., 2022. GeoThermalCloud: Machine Learning for Geothermal Resource Exploration. Journal of Machine Learning for Modeling and Computing, 3(4).

Samek, W., Montavon, G., Lapuschkin, S., Anders, C.J. and Müller, K.R., 2021. Explaining deep neural networks and beyond: A review of methods and applications. Proceedings of the IEEE, 109(3), pp.247-278.

Okoroafor, E.R., Smith, C.M., Ochie, K.I., Nwosu, C.J., Gudmundsdottir, H. and Aljubran, M.J., 2022. Machine learning in subsurface geothermal energy: Two decades in review. Geothermics, 102, p.102401.

Vesselinov, V.V., Frash, L., Ahmmed, B. and Mudunuru, M.K., 2021, June. Machine Learning to Characterize the State of Stress and its Influence on Geothermal Production. In Geothermal Rising Conference, San Diego, CA.